Journal of ELECTRONIC MATERIALS, Vol. 47, No. 12, 2018
https://doi.org/10.1007/s11664-018-6647-1

Cadmium Oxide:Titanium Dioxide Composite Based Photosensitive Diode

ABDULKERIM KARABULUT,[1,8] A. DERE,[2] ABDULLAH G. AL-SEHEMI,[3,4,5] AHMED A. AL-GHAMDI,[6] and F. YAKUPHANOGLU[7]

1.—Department of Electrical and Electronics Engineering, Faculty of Engineering, Sinop University, Sinop, Turkey. 2.—Nanoscience and Nanotechnology Laboratory, Firat University, Elazig, Turkey. 3.—Department of Chemistry, Faculty of Science, King Khalid University, P.O. Box 9004, Abha 61413, Saudi Arabia. 4.—Research Center for Advanced Materials Science, King Khalid University, P.O. Box 9004, Abha 61413, Saudi Arabia. 5.—Unit of Science and Technology, Faculty of Science, King Khalid University, P.O. Box 9004, Abha 61413, Saudi Arabia. 6.—Department of Physics, Faculty of Science, King Abdulaziz University, Jeddah 21589, Saudi Arabia. 7.—Department of Physics, Faculty of Science, Firat University, Elazig, Turkey. 8.—e-mail: akerimkara@gmail.com

Cadmium oxide:titanium dioxide (CdO:TiO_2) composite thin films with various ratios of CdO contents were prepared on *p*-type silicon semiconductor substrates by the sol–gel spin coating method. Al/CdO:TiO_2/*p*-Si/Al heterojunction devices exhibited optoelectronic device behavior due to their photocurrent under solar light illuminations. The photoresponse behavior of the diodes is controlled by changing the molar ratio of CdO to TiO_2. The fabricated CdO:TiO_2 (2:1) based device exhibited the highest photoresponse of about 7.5×10^3. The interface properties of the devices are changed with the molar ratio of CdO:TiO_2. The obtained results suggest that CdO:TiO_2 composite film/*p*-type Si structure can be used in optoelectronic applications.

Key words: Electrical properties, photodiode, CdO:TiO_2 composite, illumination effect, interfacial layer

INTRODUCTION

Titanium dioxide semiconductors have a great importance due to their favorable properties for use in electronic and optoelectronic technologies.[1–3] The TiO_2 thin films can be used to obtain different electronic devices such as semiconductor-based diodes, photodiodes or devices with optical properties, solar cells and transistors.[4–6] Some electrical and optical characteristics of TiO_2 films have been enhanced by stirring with suitable rates of metal oxides such as Al_2O_3, NiO, Fe_2O_3, SiO_2, In_2O_3, ZrO_2.[7–11]

The cadmium oxide (CdO) thin films, which are transparent conducting oxide material, have been used in a wide range of optoelectronic applications such as photovoltaics, diodes, photodevices and gas sensors due to its practical electrical and optical features.[12–15] In addition, the CdO semiconductor, which exhibits a 2.2–2.4 eV bandgap, has a direct band gap, and this case makes it attractive for optoelectronic applications.[16]

TiO_2 and CdO have been deposited on substrates by various techniques such as RF magnetron sputtering, SILAR, metal–organic chemical vapor deposition (MOCVD), thermal evaporation, physical vapor deposition (PVD) and the sol–gel process.[17–23] Among these techniques, the sol–gel technique is crucial for synthesizing metal oxide films due to some of its useful advantages such as low cost, simplicity, homogeneity and control of contents.[17]

In this study, we fabricated a heterojunction-based photosensitive device by preparing CdO:TiO_2 composite metal oxide films with various compositions with the sol–gel method. Also, electrical and optical properties of fabricated photodevices were investigated by the usage of current–voltage, transient photocurrent and capacitance–voltage

(Received May 10, 2018; accepted September 1, 2018; published online September 12, 2018)

measurements. Research on structure with a CdO-TiO_2 composite interfacial layer is novel in the literature for photodevice applications.

EXPERIMENTAL DETAILS

The Al/*p*-Si structures with CdO:TiO_2 composite interfacial layer, which is TiO_2 material combined with various molar ratios of CdO, were fabricated by using TiO_2 and CdO solutions. The titanium(IV) *n*-butoxide and cadmium acetate were used as precursors to synthesize TiO_2 and CdO materials by the sol–gel method.

Firstly, the sufficient amount of titanium(IV) *n*-butoxide was taken and dissolved in ethanol solvent. After this step, the prepared solution was stirred for 2 h, and some deionized water was added to solution. For obtaining a clear solution by arranging pH, some HNO_3 drops were added to the solution. Secondly, the nominal value of cadmium acetate was dissolved with 2-metoxyethanol and etanolamin was used for stabilizing to prepare a solution, and then prepared cadmium acetate solution was stirred using a magnetic stirrer for approximately 30 min to provide homogeneity of the solution. After preparing the solutions separately, the TiO_2 solution was added to the CdO solution to obtain a CdO:TiO_2 composite solution with various molar ratios of CdO contents (1:1), (2.1), (3.1). Before coating of prepared solutions to chemically cleaned *p*-type silicon substrate, an ohmic contact was made by the thermal evaporating method by the use of ultra pure Al metal, and it was annealed at 570°C for 5 min under nitrogen flow atmosphere after an evaporating step. After completing the ohmic contact process, CdO:TiO_2 with a different molar ratios solution was dropped onto a *p*-Si wafer, and it was covered at 1500 rpm for 40 s using by spin coating method. Then, CdO:TiO_2 covered structures were dried at 150°C for 10 min with a hot plate. Then, the prepared structures were annealed at 450°C for 1 h in air atmosphere conditions to obtain homogenous CdO:TiO_2 solid films. After the CdO:TiO_2 composite film coating process, the top metal was evaporated on CdO:TiO_2 composite film as dots of 1 mm radius through the shadow mask by using thermally evaporated Al metal. The electrical and photoelectrical characterizations were investigated by using a Fytronix 5000-ECS Electronic Device characterization system.

RESULTS AND DISCUSSION

Figure 1a, b and c indicates the measured forward and reverse bias *I–V* characteristics at room temperature and different light intensities. The measurements of *I–V* characteristics are crucial to understand electrical properties of devices based on diodes. Therefore, the electrical characteristics of the device, such as reverse bias leakage current, series resistance, barrier height and ideality factor, were determined using *I–V* measurements.[24]

Figure 1 presents a good example of the rectifying behavior of the device. Here, data is analyzed with the help of thermionic emission (TE) theory. This theory simply states that current can be calculated as a function of voltage by the following equation[25,26]:

$$I = I_s\left[\exp\left(\frac{qV - IR_s}{nkT}\right) - 1\right], \quad (1)$$

where saturation current, effective diode area, absolute temperature, ideality factor, Boltzmann constant, voltage and electron charges are represented as I_s, A, T, n, k, V and q, respectively. I_s can be calculated from the straight line intercept of $\ln(I)$ at $V = 0$, and it is given by,[27]

$$I_s = AA^*T^2\exp\left(\frac{q\Phi_b}{kT}\right), \quad (2)$$

where the effective Richardson's constant is illustrated with A^* and it is equivalent to 32 A/cm^2 K^2 for *p*-Si. Φ_b and A are the barrier height value at zero bias and metallic top contact area, respectively. The n values of devices are calculated by the use of the linear region of the *I–V* graph at forward bias. If Eqs. 1 and 2 are rearranged as the following equations, n and Φ_b can be determined[28,29];

$$n = \frac{q}{kT}\left(\frac{dV}{d(\ln I)}\right) \quad (3)$$

and

$$\Phi_b = \frac{kT}{q}\ln\left(\frac{AA^*T^2}{I_s}\right). \quad (4)$$

For the studied device, we used the Richardson constant for *p*-Si, because the doping concentration of *p*-Si is higher than that of a TiO_2 semiconductor. This suggests that the *p*-Si is dominant in the charge transport mechanism of the diode. Thus, we take the Richardson constant as 32 A/cm^2 K^2. Table I provides the ideality factor values and shows that the sample made of CdO:TiO_2 composite. The structure with 1:1 composition has the lowest ideality factor: 5.79. Beside, it is found that the values for CdO:TiO_2 composite devices change by the increase of CdO molar ratio. The calculated ideality factor values show that the diodes exhibited a non-ideal behavior due to the higher ideality factor values. In addition, the barrier height values presented at Table I were changed by the usage of different CdO contents in the composite interfacial layer. Here, it is found that the lowest barrier height value was 0.49 eV for CdO:TiO_2 composite film with 1:1 molar ratio. In other words, the high value of the ideality factor illustrates the existence of interface states originating from the oxide layer of silicon, the presence of Schottky barrier inhomogeneities, and series resistance.[30] Mohanraj et al.[31] have fabricated Ag/CdO/*p*-Si devices for investigating its electrical and optical characteristics. They found the high ideality factor values between 8.42

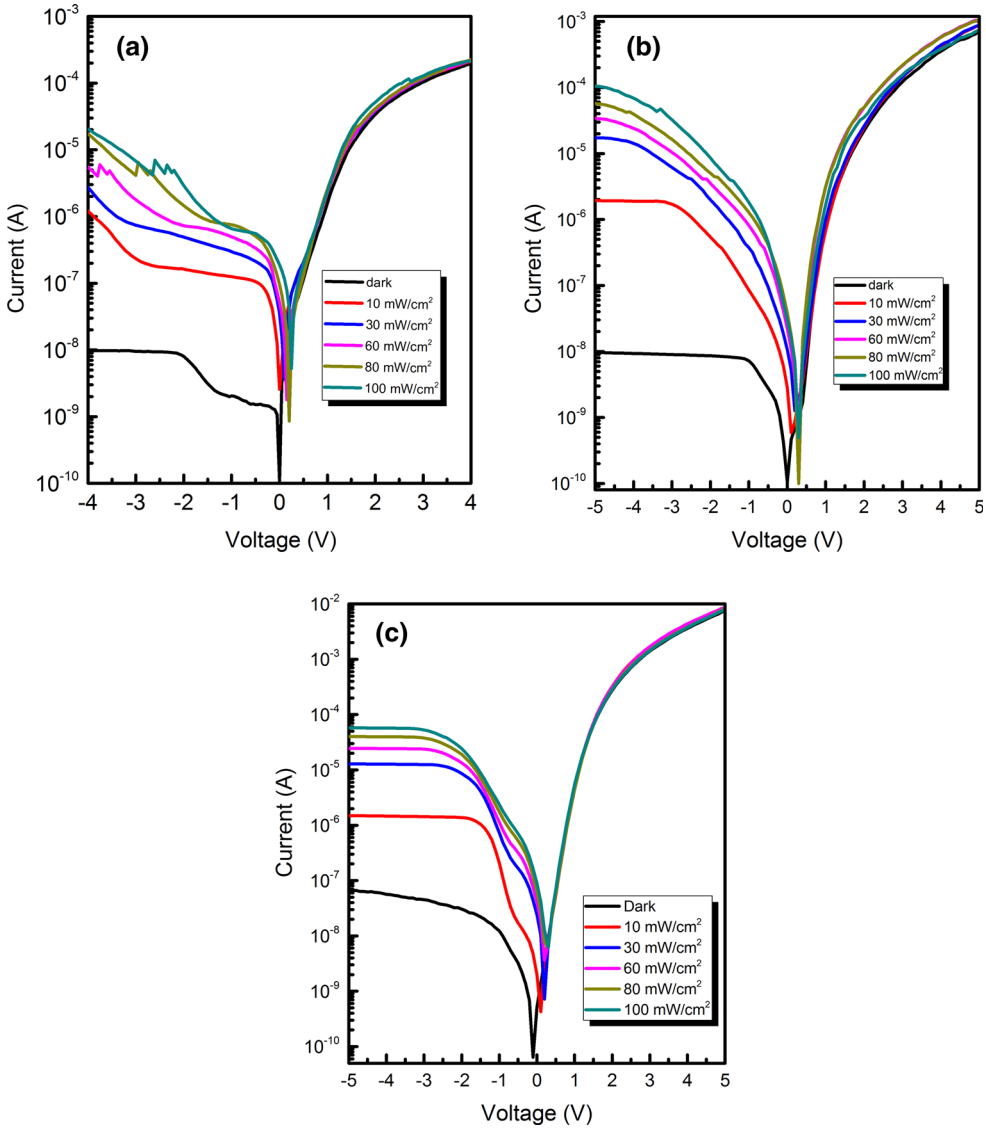

Fig. 1. Current-voltage plots of the fabricated photodiodes with various ratios of CdO contents under dark and various illumination intensities (a) CdO:TiO_2 (molar ratio 1:1), (b) CdO:TiO_2 (molar ratio 2:1), (c) CdO:TiO_2 (molar ratio 3:1).

Table I. Ideality factor and barrier height values of various doping concentrations

Molar ratios of composite	Illumination conditions	Ideality factor (n)	Barrier height (Φ_b)
CdO:TiO_2 (1:1)	Dark	5.79	0.49
	100 mW/cm^2	9.74	0.48
CdO:TiO_2 (2:1)	Dark	6.40	0.55
	100 mW/cm^2	7.96	0.52
CdO:TiO_2 (3:1)	Dark	9.31	0.50
	100 mW/cm^2	10.38	0.49

and 12.87 under dark and different light conditions and very small rectification ratios compared with the present study. Pakma et al.[32] have prepared Al/p-Si structures with TiO_2 interfacial layers. They reported ideality factor values between 2.17 and 4.61. In other research, Ocaya et al.[33] have investigated the diode with organic interfacial layers for understanding its electrical characteristics. They reported barrier height values about 0.76 eV and very high ideality factor values for diodes between 9

and 20. Based on these researches, the obtained values of fabricated diodes are sufficient in comparison with the ideality factors and barrier heights of previous studies.

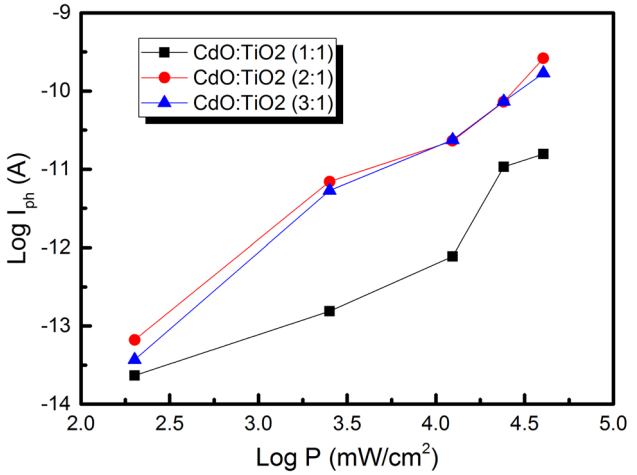

Fig. 2. Log(I_{ph}) versus log(P) plots of the photodiodes with various ratios of CdO contents (at − 4 V).

The usage of the following equation helps to determine the photoconduction mechanism of the photodiodes made of TiO_2 combined with various molar ratios of CdO contents interfacial layers[27,34];

$$I_{ph} = BP^m, \tag{5}$$

where B is constant and m is the exponent. I_{ph} and P stand for the photocurrent and solar light power, respectively. Figure 2 shows a log I_{ph} versus log P histogram.

The m value of an Al/CdO:TiO_2 (1:1)/p-Si/Al heterojunction-based photodiode was determined as 1.24 while they are found as 1.64 and 1.54 for Al/CdO:TiO_2/p-Si/Al photodiodes with (2:1) and (3:1) molar ratios of CdO materials, respectively. If the extracted value is within the $0.5 < m < 1$ condition, it can be safely stated that there is the existence of continuously localized states in the mobility-gap of structures.[35] The meaning of these results is that there is an observation of a lower density of the uninvaded trap level at higher m values, while m is greater than unity.[36] In addition to this, based on the m values, a non-linear photoconduction behavior is expected for the photoconduction mechanism of the Si-based photodiodes. The value of m is provided to understand the type of photoconducting

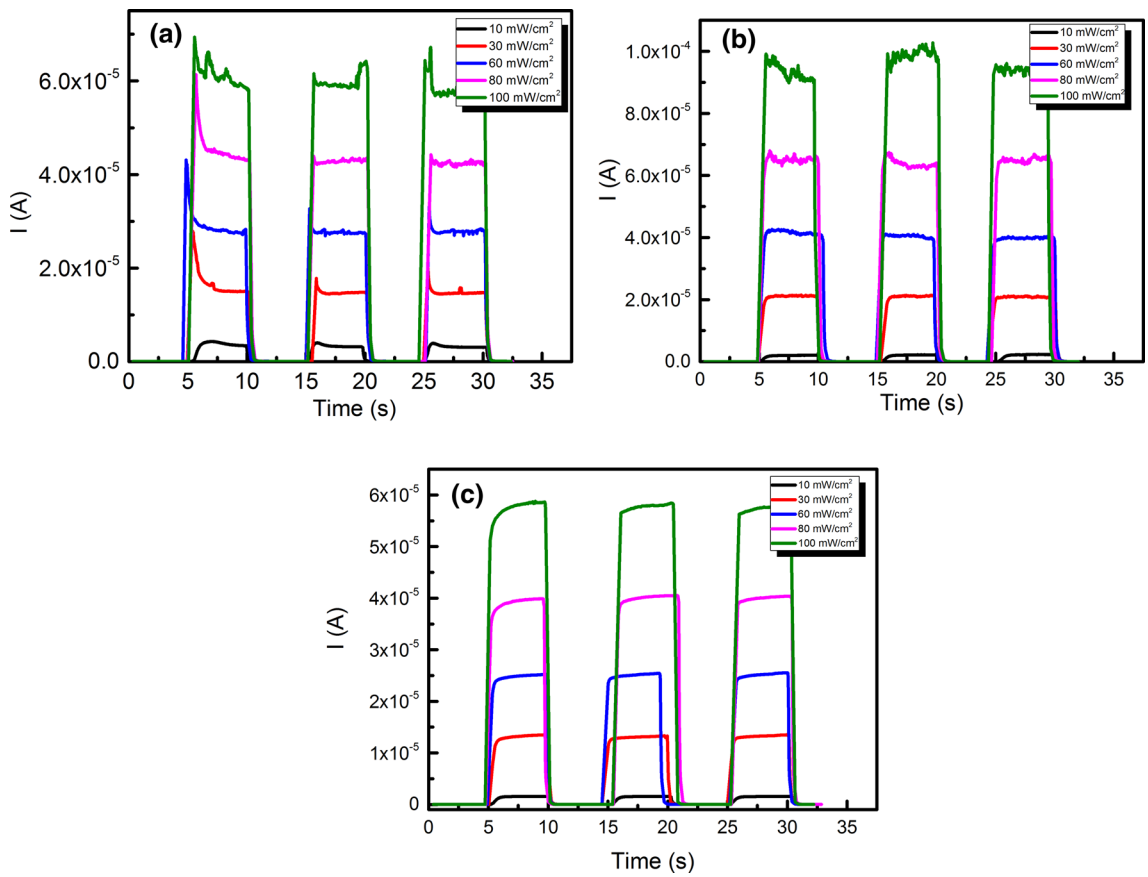

Fig. 3. Transient photocurrent-time plots of the photodiodes with various ratios of CdO contents at − 5 V. (a) CdO:TiO_2 (molar ratio 1:1), (b) CdO:TiO_2 (molar ratio 2:1), (c) CdO:TiO_2 (molar ratio 3:1) at 100 mW/cm^2.

mechanism of the fabricated photodiodes. Al-Hazmi et al.[37] investigated the ZnO:TiO_2 composite based heterojunction photodiode for its determining photovoltaic and photoconducting properties. They found 1.36 for value of m. In another research, Tataroglu et al.[10] studied to obtain electrical and optical parameters of silicon based NiO doped TiO_2 film by using the sol–gel method. The m values of prepared diodes were determined to be between 1.09 and 1.52 by them. Time for the reaction in photodiode by the effect of illumination gives the response for a fast changing optical signal, which is a crucial situation in optoelectronic devices.[38]

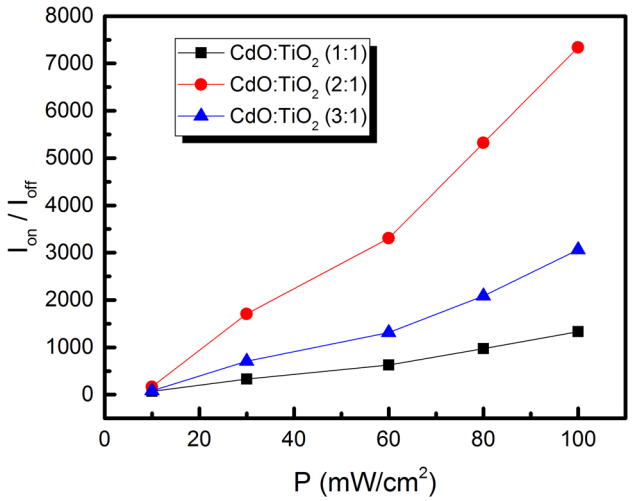

Fig. 4. Photoresponse behavior of the fabricated photodiodes with CdO:TiO_2.

Figure 3 is shown for the various light intensities with the practice of the transient photocurrent measurements to be able to make better conclusions about the photoresponse analysis of the device. Once it is turned on, the photocurrent quickly reaches a certain value, and it shows a behavior prone to the maximum value for different solar light irradiations which are ranging from 20 to 100 mW/cm^2: 20, 40, 60, 80, and 100. Then, once it is turned off, the photocurrent reverted back to its initial state. The photocurrent changes from the light on to off stem from trapping of the charge carriers in the deep levels.[39] The rise times of prepared devices were found as 0.504, 0.701 and 0.424 for (1:1), (2:1) and (3:1) molar ratios of CdO:TiO_2, respectively. While the fall times of prepared devices were found as 0.444, 0.449 and 0.413 for (1:1), (2:1) and (3:1)

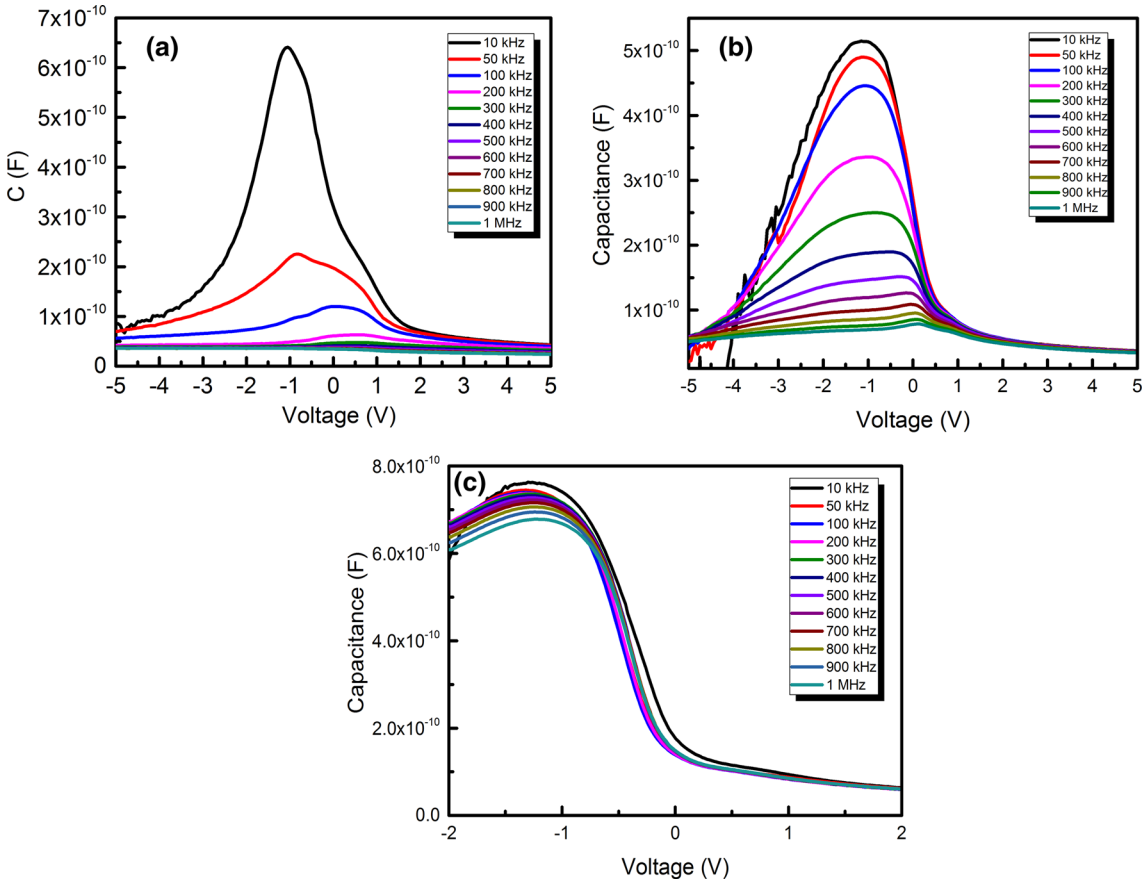

Fig. 5. Capacitance–voltage (C–V) plots of the fabricated heterojunction devices at various frequencies. (a) CdO:TiO_2 (molar ratio 1:1), (b) CdO:TiO_2 (molar ratio 2:1), (c) CdO:TiO_2 (molar ratio 3:1).

molar ratios of CdO:TiO_2, respectively. In addition to photocurrent measurements, the photoresponse, which was altered with the different solar light power intensity, is given in Fig. 4. For all measurements of fabricated photodiodes, it has been taken at 17 s and 1 s for I_{on} and I_{off}, respectively. As seen in the figure, the ratio of current I_{on}/I_{off} for the fabricated Al/CdO:TiO_2 (2:1)/*p*-Si/Al structure has the best photoresponse value, which was determined to be approximately 7342 at 100 mW/cm^2. The determined value of I_{on}/I_{off} ratio suggests that the fabricated photodiode shows a high photoresponse behavior compared with many previous studies (6411, 2262, 840).[27,34,40]

Figure 5a, b and c indicates the *C*–*V* plot of the diodes with a CdO:TiO_2 interfacial layer containing different CdO content ratios obtained at various frequencies in the range of 10 kHz to 1 MHz. As can be concluded from Fig. 5, the capacitance values of the device decrease by the increase of frequency. The applied electric field does not affect the capacitance of the diode in forward bias voltages although the capacitance changes once negative voltages are applied. In addition, the observed change decreases by the increase of frequency. This is the indication that the interface charges do not follow the signal of alternating current since there is decrease of the interface charges.[41,42] Figure 6a, b and c indicates the conductance–voltage (*G*–*V*) graphs of the Al/CdO:TiO_2/*p*-Si/Al structures which have various molar ratios of CdO contents in composite interfacial layers. It is confirmed that the conductance values increase by the increase of the frequency. The reason for this situation in the conductance behavior can be attributed to the existence of interface states and series resistance.[43] There is a peak observed in capacitance–voltage histograms due to series resistance and the existence of the interface states. Therefore, the capacitance and conductance are adjusted with the series resistance with help of the next equations.[27,44]

$$C_{adj} = \frac{\left(G_m^2 + (wC_m)^2\right)}{a^2 + (wC_m)^2} C_m \tag{6}$$

and

$$G_{adj} = \frac{\left[G_m^2 + (wC_m)^2\right]}{a^2 + (wC_m)^2} a \tag{7}$$

in the above equations, a term is equal to $[C_m - [G_m^2(wC_m)^2]]$ R_s, C_{adj} and G_{adj} terms are adjusted capacitance and adjusted conductance, respectively.

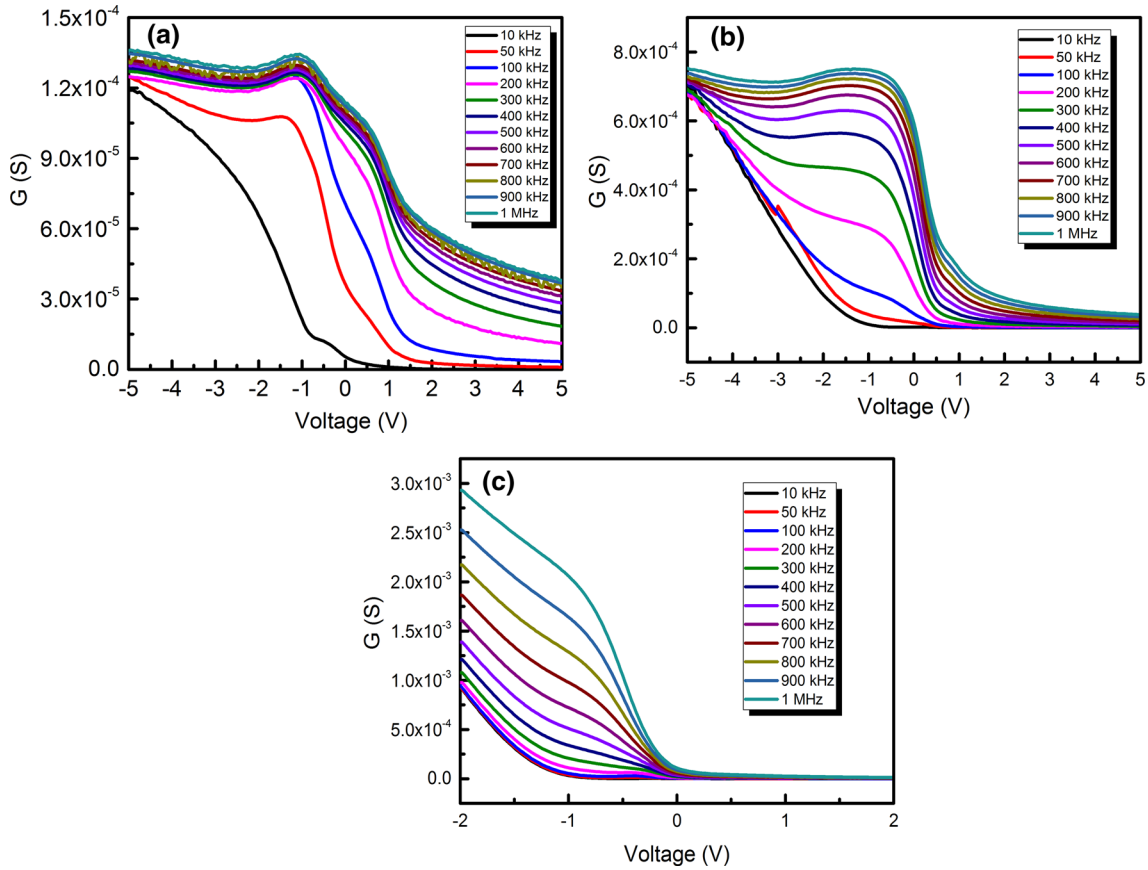

Fig. 6. Conductance–voltage (*G*–*V*) plots of the fabricated heterojunction devices at various frequencies. (a) CdO:TiO_2 (molar ratio 1:1), (b) CdO:TiO_2 (molar ratio 2:1), (c) CdO:TiO_2 (molar ratio 3:1).

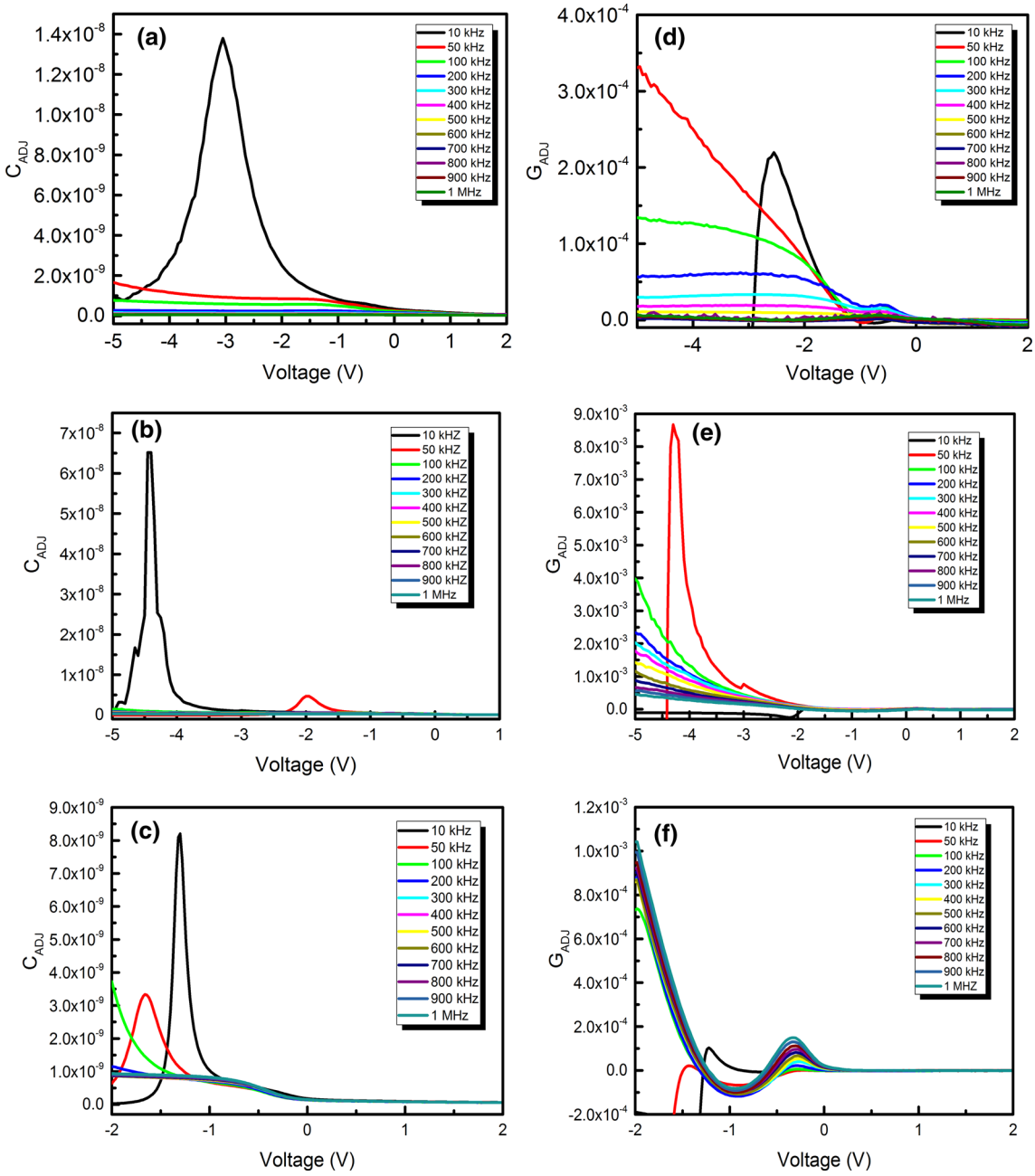

Fig. 7. Adjusted capacitance (a–c) and conductance (d–e) plots of the fabricated heterojunction devices at various frequencies for (1:1), (2:1), (3:1) molar ratios of CdO:TiO_2.

Figure 7a, b, c, d, e and f exhibits the series resistance adjusted values of capacitance and conductance at the different frequencies. As seen in Fig. 7a, b and c, it is observed that the C_{adj} changes with changing frequency in the reverse bias voltage region, in addition to this, the frequency was constant with varying voltage in the forward bias region. Furthermore, we determined a peak in the G_{adj}–V characteristics for fabricated photodiodes in the reverse bias region, and they are demonstrated in Fig. 7d, e and f. The cause of this case is based on the effect of interface states and series resistance. In addition to these, some diode parameters such as built-in potential, depletion region width and donor concentration can be determined by C^{-2}–V characteristics and shown in Fig. 8. These values was calculated for 10 kHz frequency conditions and are given in Table II.

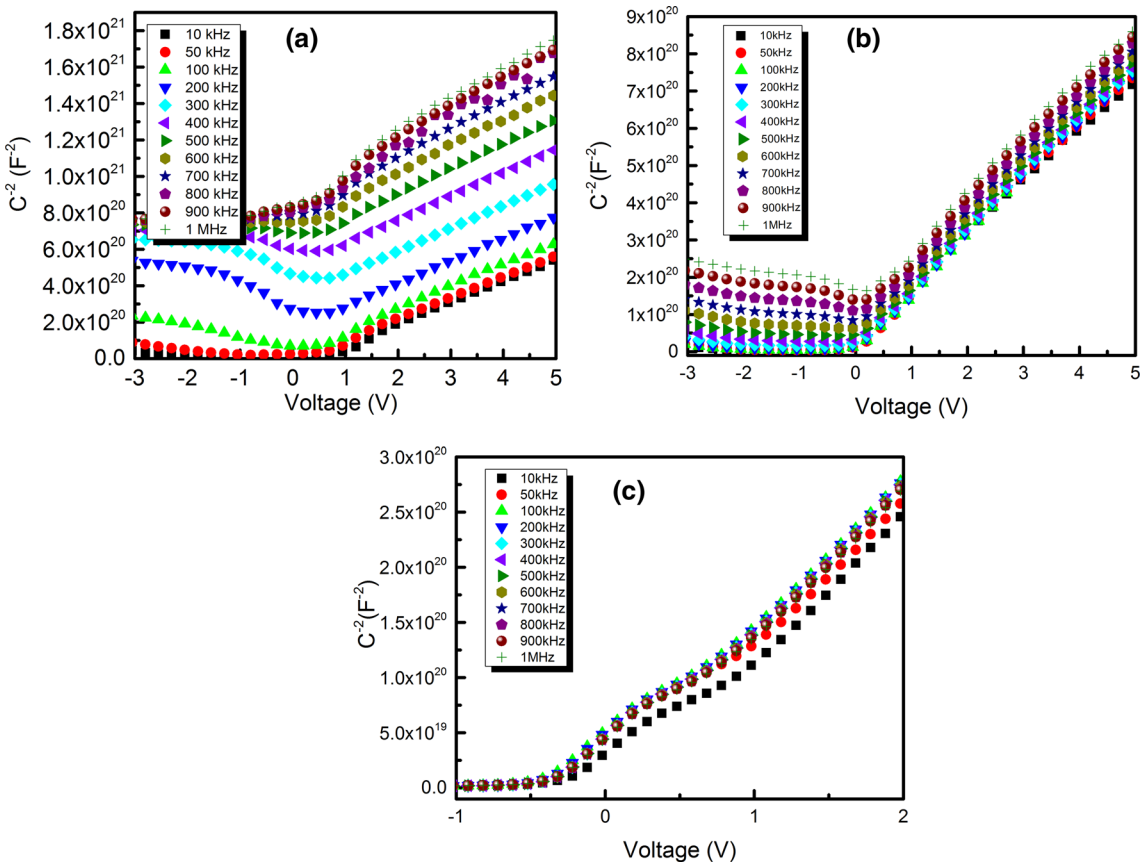

Fig. 8. C^{-2}–V plots of the fabricated heterojunction devices at various frequencies. (a) CdO:TiO_2 (molar ratio 1:1), (b) CdO:TiO_2 (molar ratio 2:1), (c) CdO:TiO_2 (molar ratio 3:1).

Table II. Some electrical parameters obtained by C^{-2}–V graphs at the 10 kHz frequency value

Molar ratios of composite	N_d (cm^{-3})	V_0 (V)	V_d (V)	W_d (m)
CdO:TiO_2 (1:1)	1.66481×10^{15}	0.222	0.247	4.423×10^{-5}
CdO:TiO_2 (2:1)	1.32358×10^{15}	0.265	0.290	5.274×10^{-5}
CdO:TiO_2 (3:1)	1.36317×10^{15}	0.172	0.198	4.370×10^{-5}

The series resistance versus voltage graphs for different fabricated photodiodes are shown in Fig. 9. In order to obtain the series resistance of the fabricated diodes with CdO:TiO_2 composite interfacial layers the following equation is used[45];

$$R_s = \frac{(G_m/wC_m)^2}{1+(G_m/wC_m)^2}\frac{1}{G_m}, \quad (8)$$

where G_m is measured conductance and C_m is measured capacitance. As seen in Fig. 9, there are strong peaks at lower frequencies, and the observed peak intensity is decreased with increasing frequency. In addition to this, the series resistances of the prepared samples were not affected by the frequency change at high frequencies and remain approximately constant. Besides, the series resistance peaks of samples with 2:1 and 3:1 molar ratios at low frequencies are more apparent. The R_s values yield a maximum in the biasing range of $-1.0 < x < -0.5$ V for samples with a 3:1 molar ratio, but there are two big peaks for samples with a 2:1 molar ratio and decrease as the frequency increases. Many researchers have investigated the effect of frequency on series resistance and reported that the series resistance decreases with increasing frequency.[46–50] Furthermore, the peak intensity of series resistance characteristics is dependent on the amount of interface states under different frequencies. Thus, we can obtain the density of interface states (D_{it}) by using an equation as follows;

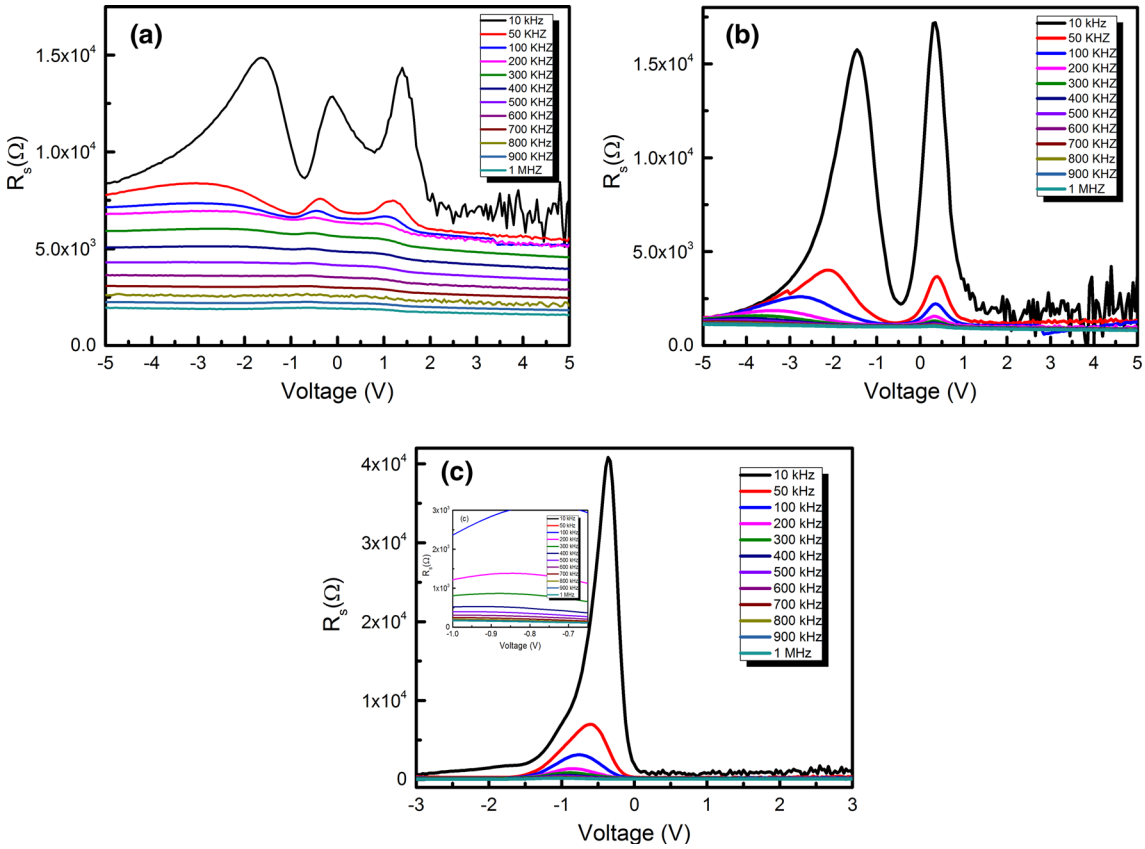

Fig. 9. Series resistance versus voltage plots of the fabricated heterojunction devices at various frequencies. (a) CdO:TiO_2 (molar ratio 1:1), (b) CdO:TiO_2 (molar ratio 2:1), (c) CdO:TiO_2 (molar ratio 3:1), (in inset: the zoomed state of the series resistance values at different frequencies).

$$D_{it} = \frac{2}{qA}\frac{\left(G_{\mathrm{adj}}/w\right)_{\max}}{\left[\left(\frac{G_{\max}}{wC_{\mathrm{ox}}}\right)^2 + \left(\frac{1-C_{\mathrm{m}}}{C_{\mathrm{ox}}}\right)^2\right]}, \qquad (9)$$

where $(G_{\mathrm{adj}}/w)\max$, w, A, C_{ox} and C_{m} terms stand for the measured conductance, angular frequency, the area of the diode, the capacitance of the insulator layer and the measured capacitance, respectively. The calculated interface state densities for fabricated diodes, which are a function of frequency, are given in Fig. 10. As seen in figure, D_{it} values decrease with increasing frequency for devices which are 1:1 and 2:1 molar ratios of CdO:TiO_2, and increase with increasing frequency for 3:1 molar ratios of the CdO:TiO_2 diode. It is seen that the interfacial state densities are close to constant at the higher frequencies. This behavior is attributed to the interface state charges that can not follow the ac signal at high frequencies.[42,46,51,52] On the other hand, the high values of D_{it} are one of the crucial causes of the non-ideal behavior of diodes.[53]

CONCLUSIONS

CdO:TiO_2 composite thin films with various CdO contents were prepared by the sol–gel technique. Photodiode-based Al/CdO:TiO_2 composite/p-Si/Al structures were fabricated by the spin coating method. The electrical parameters of the fabricated diodes were investigated from I–V and C–V characteristics. Rectifying behavior was observed for the fabricated diodes and ideality factors of diodes were calculated higher than unity. Furthermore, the illumination effects for electrical properties of the diodes were determined under varying solar light power intensities. The experimental results exhibit that the electronic and optoelectronic characteristics of the prepared structures are changed with varying CdO contents in an interfacial composite layer. It is seen that the fabricated diodes are sensitive to light power intensity strongly. Finally, it is reported that the fabricated structures in this present work might be used as photodiodes in optoelectronic applications.

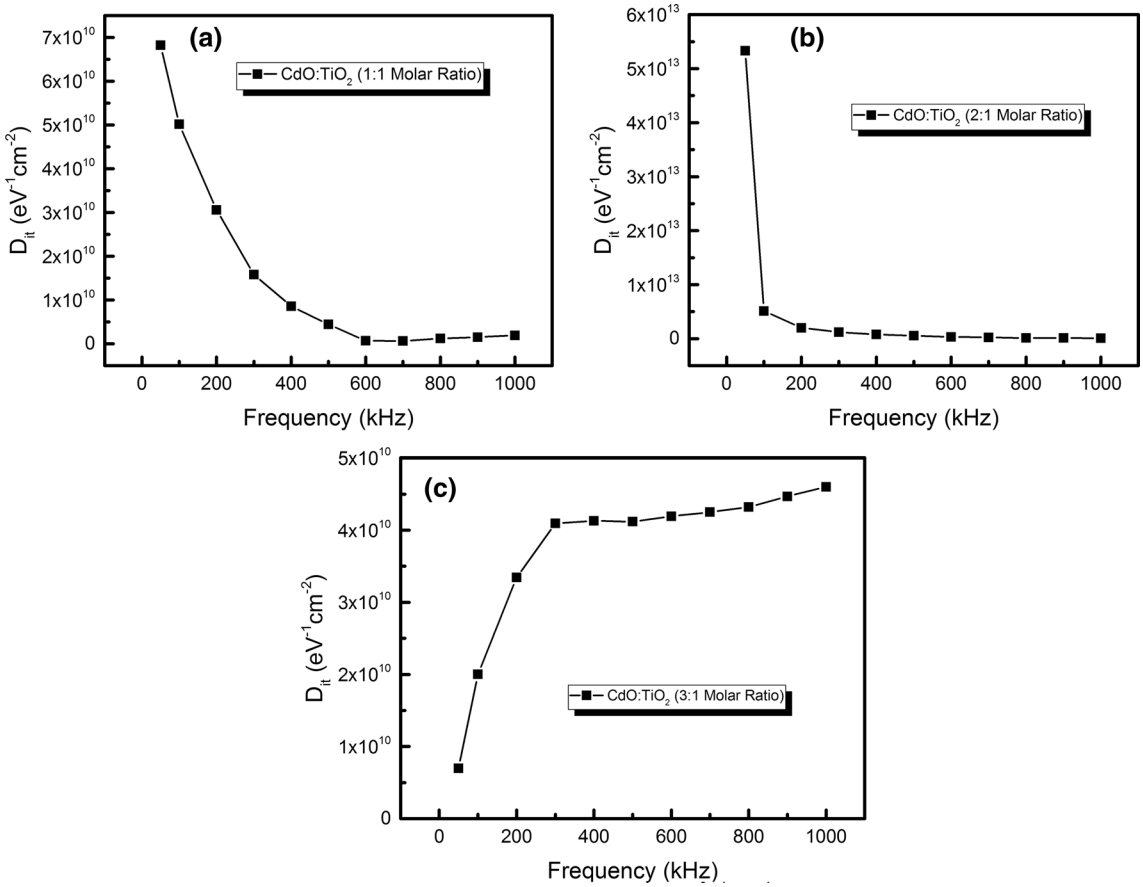

Fig. 10. Plots of D_{it} value versus frequency of the devices. (a) CdO:TiO_2 (molar ratio 1:1), (b) CdO:TiO_2 (molar ratio 2:1), (c) CdO:TiO_2 (molar ratio 3:1).

ACKNOWLEDGEMENTS

The authors would like to acknowledge the support of the King Khalid University for this research through a Grant RCAMS/KKU/007-18 under the (Research Center for Advanced Materials Science) at King Khalid University, Kingdom of Saudi Arabia.

REFERENCES

1. B. Choudhuri, A. Mondal, S.M.M.D. Dwivedi, and M. Henini, *J. Alloys Compd.* 712, 7 (2017).
2. P.C. Wang, C.L. Lin, Y.K. Su, P.C. Chien, G.S. Huang, S.C. Kuo, and G.C. Lyu, *Thin Solid Films* 570, 273 (2014).
3. A.H. Chiou, S.D. Wu, R.C. Hsiao, and C.Y. Hsu, *Thin Solid Films* 616, 116 (2016).
4. M.E. Harb, S. Ebrahim, M. Soliman, and M. Shabana, *J. Electron. Mater.* 47, 353 (2018).
5. M. Hironaka, T. Toyoda, K. Hori, Y. Ogomi, S. Hayase, and Q. Shen, *J. Mod. Phys.* 8, 522 (2017).
6. V.N. Kruchinin, T.V. Perevalov, V.V. Atuchin, V.A. Gritsenko, A.I. Komonov, I.V. Korolkov, L.D. Pokrovsky, C.W.E.I. Shih, and A. Chin, *J. Electron. Mater.* 46, 6089 (2017).
7. J. Araña, O.G. Diaz, M.M. Saracho, J.M.D. Rodriguez, J.A.H. Melian, and J.P. Pena, *Appl. Catal. B* 36, 113 (2002).
8. C. Anderson and A.J. Bard, *J. Phys. Chem. B* 5647, 2611 (1997).
9. X. Fu, L.A. Clark, Q. Yang, and M.A. Anderson, *Environ. Sci. Technol.* 30, 647 (1996).
10. A. Tataroğlu, A. Al-Sehemi, M. Ilhan, A.A. Al-Ghamdi, and F. Yakuphanoglu, *Silicon* 10, 913 (2017).
11. S.K. Poznyak, D.V. Talapin, and A.I. Kulak, *J. Phys. Chem. B* 105, 4816 (2001).
12. S. Sharma, S. Chaudhary, and A. Kapoor, *J. Sol-Gel. Sci. Technol.* 82, 315 (2017).
13. M. Ravikumar, V. Ganesh, M. Shkir, R. Chandramohan, K.D. Arun, S. Valanarasu, A. Kathalingam, and S. Alfaify, *J. Mol. Struct.* 1160, 311 (2018).
14. M. Ravikumar, R. Chandramohan, S. Valanarasu, and R. Manogowri, *Inorg. Nano-Metal Chem.* 47, 1495 (2017).
15. J.K. Rajput, T.K. Pathak, V. Kumar, and L.P. Purohit, *Appl. Surf. Sci.* 409, 8 (2017).
16. S.V. Kahane, R. Sasikala, B. Vishwanadh, V. Sudarsan, and S. Mahamuni, *Int. J. Hydrogen Energy* 38, 15012 (2013).
17. M. Thirumoorthi and J.T. Joseph, *Integr. Med. Res.* 4, 39 (2016).
18. D.G. Cahill and T.H. Allen, *Appl. Phys. Lett.* 65, 309 (1994).
19. M.O. Abou-helal and W.T. Seeber, *Appl. Surf. Sci.* 195, 53 (2002).
20. Q. Wang, X. Yang, D. Liu, and J. Zhao, *J. Alloys Compd.* 527, 106 (2012).
21. B. Yin, H. Zhang, Y. Qiu, Y. Luo, Y. Zhao, and L. Hu, *Nano Energy* 40, 440 (2017).
22. P. Velusamy, R.R. Babu, K. Ramamurthi, E. Elangovan, and J. Viegas, *J. Alloys Compd.* 708, 804 (2017).
23. M.A. Yıldırım and A. Ateş, *Sensors Actuators A Phys.* 155, 272 (2009).
24. K. Ejderha, A. Karabulut, N. Turkan, and A. Turut, *Silicon* 9, 395 (2016).
25. M. Ilhan, *J. Mater. Electron. Dev.* 1, 15 (2017).

26. W.C. Huang, T.C. Lin, C.T. Horng, and Y.H. Li, *Mater. Sci. Semicond. Process.* 16, 418 (2013).
27. B. Anwer Gozeh, A. Karabulut, A. Yildiz, and F. Yakuphanoglu, *J. Alloys Compd.* 732, 16 (2018).
28. İ. Orak, A. Kocyigit, and A. Turut, *J. Alloys Compd.* 691, 873 (2017).
29. İ. Orak, *Solid State Commun.* 247, 17 (2016).
30. S. Altindal, *J. Mater. Electron. Dev.* 1, 42 (2017).
31. K. Mohanraj, D. Balasubramanian, J. Chandrasekaran, and B. Babu, *J. Mater. Sci. Mater. Electron.* 28, 7749 (2017).
32. O. Pakma, N. Serin, T. Serin, and Ş. AltIndal, *J. Sol-Gel. Sci. Technol.* 50, 28 (2009).
33. R.O. Ocaya, A. Dere, A.G. Al-Sehemi, A.A. Al-Ghamdi, M. Soylu, and F. Yakuphanoglu, *Phys. E Low-Dimens. Syst. Nanostruct.* 93, 284 (2017).
34. F. Yakuphanoglu, *Compos. Part B Eng.* 92, 151 (2016).
35. M. Cavas, A.A.M. Farag, Z.A. Alahmed, and F. Yakuphanoglu, *J. Electroceram.* 31, 298 (2013).
36. A. Mekki, R.O. Ocaya, A. Dere, A.A. Al-ghamdi, K. Harrabi, and F. Yakuphanoglu, *Synth. Met.* 213, 47 (2016).
37. F.E. Al-Hazmi and F. Yakuphanoglu, *Silicon* 10, 781 (2018).
38. N.M. Khusayfan, A.A. Al-ghamdi, and F. Yakuphanoglu, *J. Alloys Compd.* 663, 796 (2016).
39. O. Cicek, H.U. Tecimer, S.O. Tan, H. Tecimer, S. Altindal, and I. Uslu, *Compos. Part B Eng.* 98, 260 (2016).
40. B.A.H. Ameen, A. Yildiz, W.A. Farooq, and F. Yakuphanoglu, *Silicon* (2017). https://doi.org/10.1007/s12633-017-9656-4.
41. V.R. Reddy, A. Umapathi, and L.D. Rao, *Curr. Appl. Phys.* 13, 1604 (2013).
42. A. Turut, A. Karabulut, K. Ejderha, and N. Bıyıklı, *Mater. Res. Express* 2, 46301 (2015).
43. A. Turut, A. Karabulut, K. Ejderha, and N. Bıyıklı, *Mater. Sci. Semicond. Process.* 39, 400 (2015).
44. E.H. Nicollian, A. Goetzberger, and A.D. Lopez, *Solid State Electron.* 12, 937 (1969).
45. R.K. Gupta, Y. Al-Turki, F. El-Tantawy, F. Yakuphanoglu, and A.A. Al-Ghamdi, *J. Mater. Electron. Dev.* 1, 11 (2017).
46. A.S. Dahlan, A. Tataroglu, A.A. Al-Ghamdi, A.A. Al-Ghamdi, S. Bin-Omran, Y. Al-Turki, F. El-Tantawy, and F. Yakuphanoglu, *J. Alloys Compd.* 646, 1151 (2015).
47. A. Mekki, A. Dere, K. Mensah-Darkwa, A. Al-Ghamdi, R.K. Gupta, K. Harrabi, W.A. Farooq, F. El-Tantawy, and F. Yakuphanoglu, *Synth. Met.* 217, 43 (2016).
48. N. Aslan, M.M. Koç, A. Dere, B. Arif, M. Erkovan, A.G. Al-Sehemi, A.A. Al-Ghamdi, and F. Yakuphanoglu, *J. Mol. Struct.* 1155, 813 (2018).
49. M. Soylu, M. Cavas, A.A. Al-Ghamdi, Z.H. Gafer, F. El-Tantawy, and F. Yakuphanoglu, *Sol. Energy Mater. Sol. Cells* 124, 180 (2014).
50. S. Zeyrek, E. Acaroğlu, Ş. Altindal, S. Birdoğan, and M.M. Bülbül, *Curr. Appl. Phys.* 13, 1225 (2013).
51. E.H. Rhoderick and R.H. Williams, *Metal-Semiconductor Contacts* (Oxford: Clarendon Press, 1988).
52. A. Karabulut, A. Türüt, and Ş. Karataş, *J. Mol. Struct.* 1157, 513 (2018).
53. A.G. Al-Sehemi, K. Mensah-Darkwa, A.A. Al-Ghamdi, M. Soylu, R.K. Gupta, and F. Yakuphanoglu, *Spectrochim Acta Part A Mol. Biomol. Spectrosc.* 180, 110 (2017).